Short Communication

In situ Investigation of the Initial Stages of AZ91D Magnesium Alloy Biodegradation in Simulated Body Fluid

Emmanuel Mena-Morcillo[1], Lucien Veleva[1,*], David O. Wipf[2]

[1] Departamento de Física Aplicada, Centro de Investigación y Estudios Avanzados del Instituto Politécnico Nacional (CINVESTAV-IPN) – Unidad Mérida, Carr. Ant. a Progreso Km. 6, 97310, Mérida, Yucatán, México.
[2] Department of Chemistry, Mississippi State University, Mississippi State, MS 39762, USA.
[*]E-mail: veleva@cinvestav.mx

Magnesium alloys have recently been considered as very promising materials for biodegradable and resorbable medical implants. Despite this work, there are very few studies that use micro-electrochemical techniques for characterizing these alloys in a physiological environment. Here, the scanning electrochemical microscope (SECM) is used to map and assess the initial stages of electrochemical degradation of AZ91D magnesium alloy when exposed to simulated body fluid (SBF). The SECM feedback mode was used to monitor physical changes in the AZ91D surface, while the substrate-generation/tip-collection mode (SG/TC) was used to map the hydrogen evolution flux caused by magnesium corrosion. The results indicate dynamic electrochemical activity on the AZ91D substrate at short exposure times, indicating rapid pit nucleation and changes in hydrogen evolution intensity. In addition, SECM maps were correlated with alloy microstructure by optical and SEM-EDS images

1. INTRODUCTION

Investigation of magnesium alloys as biomaterials has recently increased due to their good mechanical properties and because of their biocompatibility and that they can be resorbed in the human body [1-4]. However, these alloys present high degradation rates when they are exposed to physiological fluids, thus hindering their clinical implementation. How fast is the degradation of Mg alloys? It depends directly on the microstructure of each alloy [5]. Among available commercial magnesium alloys, AZ91D is an interesting and suitable material for medical implant applications [6-9]. The AZ91D microstructure is typically composed of an α-matrix, the β-phase (Mg$_{17}$Al$_{12}$), and

various intermetallic particles, such as Al_8Mn_5 [10]. These β-phase and intermetallic regions present less negative corrosion potentials compared to the α-matrix, leading to preferential corrosion of the matrix in any galvanic couple [11,12]. Thereby, pit nucleation will take place in areas where those heterogeneities are adjacent to the α-phase [13,14]. Moreover, the volume fraction of β-phase will affect AZ91D degradation rate by acting as a barrier or as a galvanic cathode [15,16].

A better and more complete understanding of the degradation of Mg alloy under relevant physiological conditions requires investigation with different techniques to describe the phenomena involved in this process. Scanning electrochemical microscopy (SECM) is suitable to monitor corrosion processes *in situ* at high spatial and electrochemical resolution [17-20]. SECM techniques have been successfully applied to study Mg alloys in various solutions [21]. For instance, Souto et al. [22] studied the concentration distribution of Mg^{2+} at an AZ63 alloy in 1 mM NaCl solution with potentiometric SECM. Another example is the investigation by Tefashe et al. [23] using substrate-generation/tip-collection SECM, which allowed the detection and quantification of H_2 flux produced by an AM50 alloy exposed to 0.6 M NaCl solution. Further, Liu et al. [24] explored the localized corrosion of AM60 and AMCe1 alloys in 0.1 M and 0.3 M NaCl solutions through SECM feedback mode.
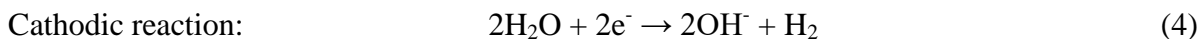
Most SECM studies of magnesium alloys have not been conducted in physiological environments [22-32]. In this work, simulated body fluid (SBF) was selected as a test media due to its stability and ionic concentration near to that of blood plasma [33]. The chloride ions present in SBF promote pitting corrosion on Mg alloys through the following reactions [34]:

$$Mg + 2Cl^- \rightarrow MgCl_2 \qquad\qquad (1)$$

$$Mg(OH)_2 + 2Cl^- \rightarrow MgCl_2 + 2OH^- \qquad\qquad (2)$$

whereas calcium and phosphate ions may form partially protective corrosion product layers [35,36]. In one study, Jamali et al [37] used SECM to examine AZ31 Mg alloy corrosion in SBF, however, the authors did not focus on how the alloy surface changes with time. Hence, one goal of the present study is to follow the evolution of AZ91D magnesium alloy surface activity in its first stages of corrosion in SBF.

For SECM feedback mode, it is important to use an appropriate tip electrode and redox mediator species to prevent measurement artefacts. Redox mediators based on Fe(II) species are suitable for use with Mg alloys due to their oxidation potential. Ferrocenemethanol (FcMeOH) has been the most commonly used mediator in previous works [24,27,28,37]. Further, Dauphin-Ducharme et al. [28] reported that carbon-fiber microelectrodes perform better than platinum for feedback measurements, since parasitic currents related to the hydrogen oxidation reaction (HOR) are inhibited at carbon electrodes. Therefore, carbon-fiber-based probes and FcMeOH should be employed to achieve more accurate measurements when Mg alloys are studied by feedback mode.

It is well known that Mg and its alloys release hydrogen as a product of the cathodic partial corrosion reaction when they are exposed to aqueous environments:

Anodic reaction: $\quad\quad\quad\quad\quad\quad\quad\quad$ $Mg \rightarrow Mg^{2+} + 2e^-$ $\quad\quad\quad\quad\quad\quad\quad\quad$ (3)

Cathodic reaction: $\quad\quad\quad\quad\quad\quad\quad$ $2H_2O + 2e^- \rightarrow 2OH^- + H_2$ $\quad\quad\quad\quad\quad\quad$ (4)

For SECM detection purposes the hydrogen produced at the cathodic sites on the Mg surface, can be oxidized at a platinum tip microelectrode as follows:

Reaction at the platinum tip: $\quad\quad\quad$ $H_2 \rightarrow 2H^+ + 2e^-$ $\quad\quad\quad\quad\quad\quad\quad\quad$ (5)

This possibility has been exploited by other researchers to study the flux of H_2 gas evolving from the surface of Mg-based materials [23,26,29,31,37]. However, to avoid interference from the simultaneous reduction of dissolved oxygen, the Pt electrode potential must be between -0.05 V and 0.0 V (vs Ag/AgCl).

The aim of this work is to investigate by SECM the initial stages of the local electrochemical degradation behavior of AZ91D surface immersed in simulated body fluid (SBF). Feedback and substrate generation/tip collection (SG/TC) modes were employed to characterize the activity on AZ91D surface and to detect hydrogen evolution produced by its degradation, respectively. The obtained SECM maps were correlated with optical and SEM images. The results of this work are expected to be useful for researchers exploring the relevance of using scanning micro-electrochemical methods to assess the *in vitro* biodegradation of magnesium alloys. To our knowledge, no other research on the bio-corrosion of AZ91D alloy in SBF by means of SECM has been previously undertaken.

2. EXPERIMENTAL

2.1. Sample and solution preparation

The AZ91D magnesium alloy (nominal wt%: 9-Al, 1-Zn, 0.3-Mn, and balance Mg) was manufactured by an ingot casting process and supplied by Magnesium Elektron Ltd (Swinton, England) as a 2 mm thick sheet. The alloy sheet was cut into strips and then embedded in epoxy resin to expose a working area of approximate 230 μm × 210 μm. Before each experiment the sample was abraded with 400, 800, and 1200 grit SiC papers, using ethanol as lubricant, and then polished with an ethanolic suspension of 0.3 μm alumina. After polishing, it was sonicated in ethanol for 2 min, to remove any residual alumina and dried in air.

The simulated body fluid employed in this work was prepared using analytical grade reagents (NaCl, NaHCO₃, Na₂CO₃, KCl, K₂HPO₄·3H₂O, MgCl₂·6H₂O, HEPES, CaCl₂,Na₂SO₄, NaOH), and ultrapure deionized water (18.2 MΩ cm), following a literature procedure [33]. Ferrocenemethanol (FeMeOH, Across Organics, New Jersey, USA), the redox mediator for SECM feedback mode, was used at a 2 mM concentration in the SBF.

2.2. Instrumentation

Cyclic voltammograms were obtained with a BAS 100B workstation and preamplifier (Bioanalytical Systems, Indiana, USA). Scanning electrochemical microscopy measurements were carried out with the home-made instrument described previously [17,38]. Briefly, a bipotentiostat (EI-400 Ensman Instruments, Indiana, USA) was used as electrochemical interface to control tip potential. Scanning was done using a controller device, which allows 3D movement through inchworm piezoelectric motors (Burleigh Instruments Inc., New York, USA). A video microscope assisted in positioning the tip close to the surface.

Optical images of the sample surface were acquired before and after experiments with an Olympus BH2 model optical microscope (Olympus Co., Tokyo, Japan) and a ToupTek CMOS camera and ToupView software (ToupTek Photonics Co. Ltd, Zhejiang, China). The microstructure of the alloy was investigated by scanning electron microscopy (SEM-EDS, Philips XL-30, Amsterdam, The Netherlands).

2.3. SECM measurements procedure

2.3.1. Microelectrodes

Platinum wire, supplied by Alfa Aesar (Ward Hill, MA, USA), and carbon fiber from Amoco Performance Products Inc. (Chicago, IL, USA) with 10 μm and 7 μm diameter, respectively, were used for microelectrode fabrication as described elsewhere [39]. In brief, Pt wire was sealed into a borosilicate glass capillary with an outer diameter of 1.5 mm and inner diameter of 0.86 mm (Sutter Instrument, Novato, CA, USA). Then the tip end was sharpened and polished to produce a ratio of insulator to glass (RG) of about seven. Carbon-fiber (CF) electrodes were constructed by inserting the fiber into a borosilicate glass capillary (1.0 mm O.D, 0.30 mm I.D., Sutter Instrument), pulled by a micropipette puller (Model P-87, Sutter Instrument), sealed, and then slightly polished to RG ≈ 5.

2.3.2 Experiments setup

For all SECM experiments, a Pt wire (0.7 mm diameter, Alfa Aesar, Ward Hill, MA, USA) was used as an auxiliary electrode, and a Ag/AgCl/KCl (3 M) reference electrode was employed to complete the electrochemical cell. The reference electrode was prepared using a 0.6 mm diameter Ag wire (Goodfellow Cambridge Ltd, Huntingdon, England), and following a well-established method [40]. In this work, all potentials are referred to the reference electrode mentioned above, and all substrates were left at OCP conditions.

Positioning of the platinum microelectrode tip to the electrode surface was accomplished by applying -0.65 V to reduce dissolved oxygen naturally present in the SBF. Positioning the carbon-fiber microelectrode tip used a potential of +0.50 V, corresponding to the ferrocenemethanol mediator diffusion-limited oxidation current. Both approach curves were done with the tip above the insulating resin to produce a negative feedback current-distance response. Once positioned, the tip was set at a

constant height from the sample surface (7 μm for the platinum microelectrode and 5 μm for carbon-fiber microelectrode), and then the X-Y plane was scanned at the indicated potential for each experiment. All experiments were carried out with a scan rate of 20 μm/s and a gain of 1 nA/V. An approximate scan time of 20 min was required to acquire the SECM images. Thus, 3D maps were obtained, with the X-Y axes representing spatial coordinates parallel to the alloy surface and the Z coordinate indicating the tip current response. All experiments were repeated to ensure a reproducible result.

3. RESULTS AND DISCUSSION

3.1. Microelectrodes characterization

To verify the correct operation of both microelectrodes employed in this study, cyclic voltammetry of 2 mM ferrocenemethanol in SBF was performed. The CV data also provides the steady steady-state diffusion-controlled limiting current ($i_{T,\infty}$), which results from the oxidation reaction of ferrocene to ferrocinium (FcMeOH $\rightleftharpoons$ e$^-$ + FcMeOH$^+$). The limiting current ($i_{T,\infty}$) is a function of microelectrode radius (a), ferrocenemethanol concentration (c) and its diffusion coefficient (D), as shown by the following equation:

$$i_{T,\infty} = 4FDca \qquad (6)$$

Comparing the current measured at the tip (in SECM feedback mode) is used to determine if substrate exhibit positive, negative or intermediate kinetic features. Figure 1 presents the CV data of the platinum and carbon-fiber microelectrodes.
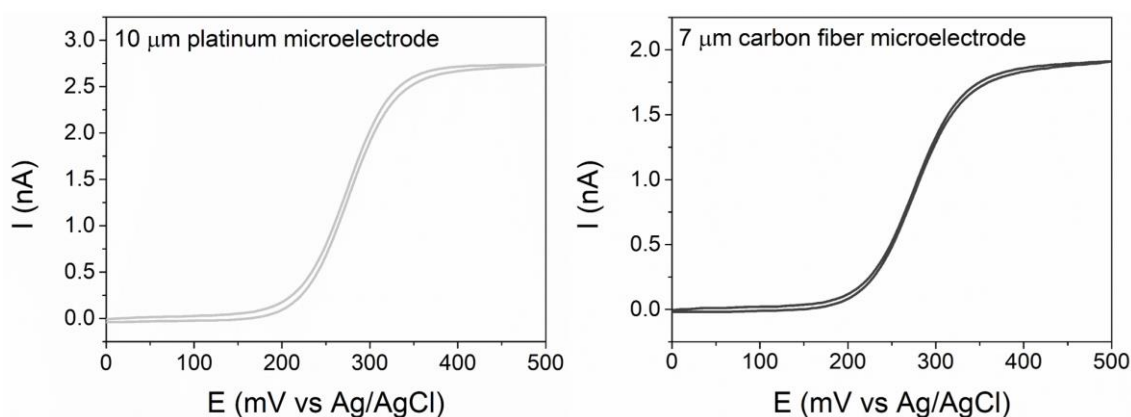

Figure 1. CVs of both the platinum and carbon-fiber microelectrodes recorded in SBF/2 mM FcMeOH ($i_{T,\infty}$ = 2.67 nA, and $i_{T,\infty}$ = 1.87 nA respectively) at a scan rate of 30 mV/s.

3.2. Feedback mode maps

Figure 2 shows maps of electrochemical activity on AZ91D substrate at different times of exposure to SBF/2 mM FcMeOH. Optical microscope images compare the alloy surface before and after the experiments.
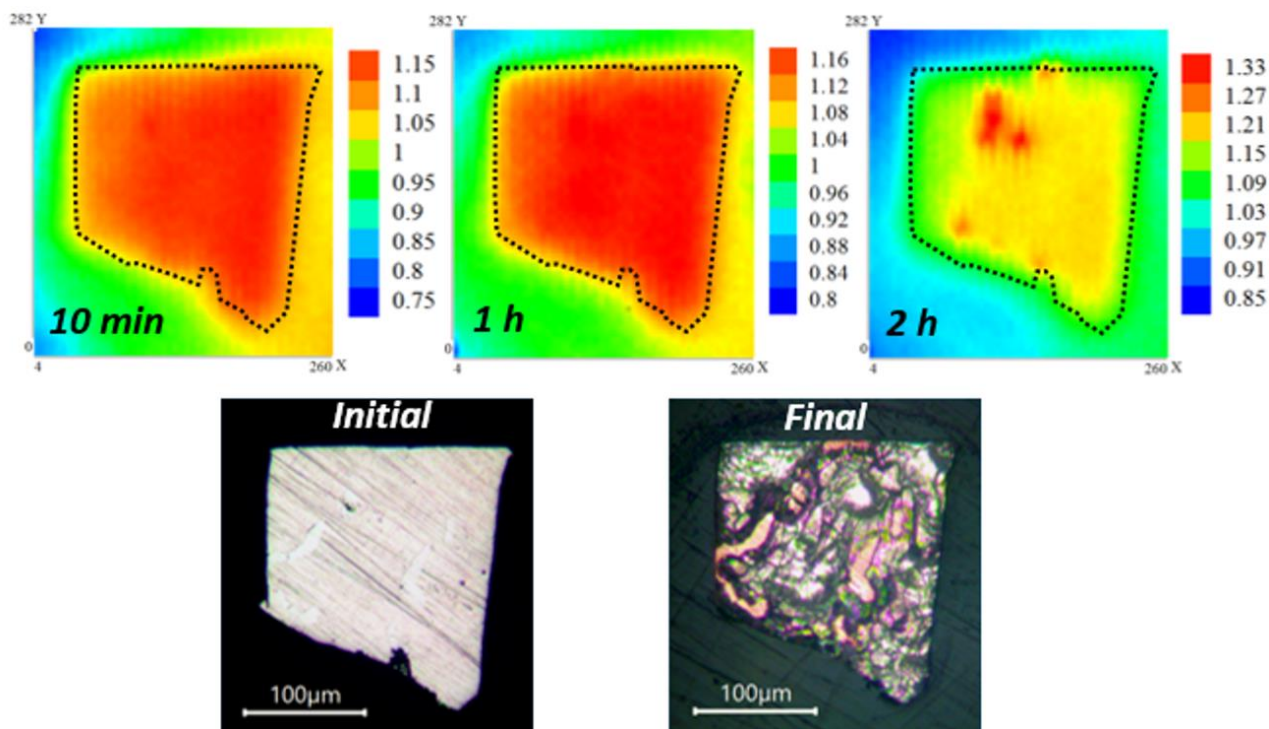
Figure 2. Top: Maps of AZ91D in SBF/2 mM FcMeOH recorded in feedback mode with the carbon-fiber microelectrode (+0.50 V) at different exposure times. Scan dimensions: 260 μm × 280 μm. Color scales are tip current in nA. Dotted outline on maps indicates metal-insulator border. Bottom: Optical images before and after the experiment..

After only 10 min of immersion the surface was uniformly active for the regeneration of ferrocenium methanol ion to ferrocenemethanol. Note that the current (i_T) measured during this time is less than the steady steady-state diffusion-controlled current ($i_T < 1.87$ nA; Figure 1), thus reflecting a limitation in electron-transfer rate across the substrate surface.

This intermediate behavior, between completely positive and completely negative feedback, has been reported previously [28], and it was attributed to the porosity of an oxide layer formed on the surface of AM50 Mg alloy. Such a layer was active during the corrosion process, allowing penetration of the FcMeOH$^+$ ion through it.

After 1 h of immersion, the corresponding map shows that the current values range remained, so the electrochemical activity of the surface was considered as still uniform. Finally, after 2 h of immersion, a noticeable localized behavior was detected. At this time, the current value increased in the most active sites. Summarizing, uniform activity was recorded at the first 10 min and 1 h, and localized behavior was finally observed at 2 h, which was related to the nucleation of the first pits.

This attack is characteristic of Cl$^-$ ions [41], which are present in the SBF solution. Also, it should be noted from optical images than pitting is localized near a second phase. This will be further discussed in SEM-EDS analysis section.

3.3. SEM-EDS analysis

Figure 3 presents SEM images of AZ91D surface acquired before and after 2 h of exposure to SBF solution. Table 1 shows EDS analysis on specific zones observed on the surface of an unexposed sample.
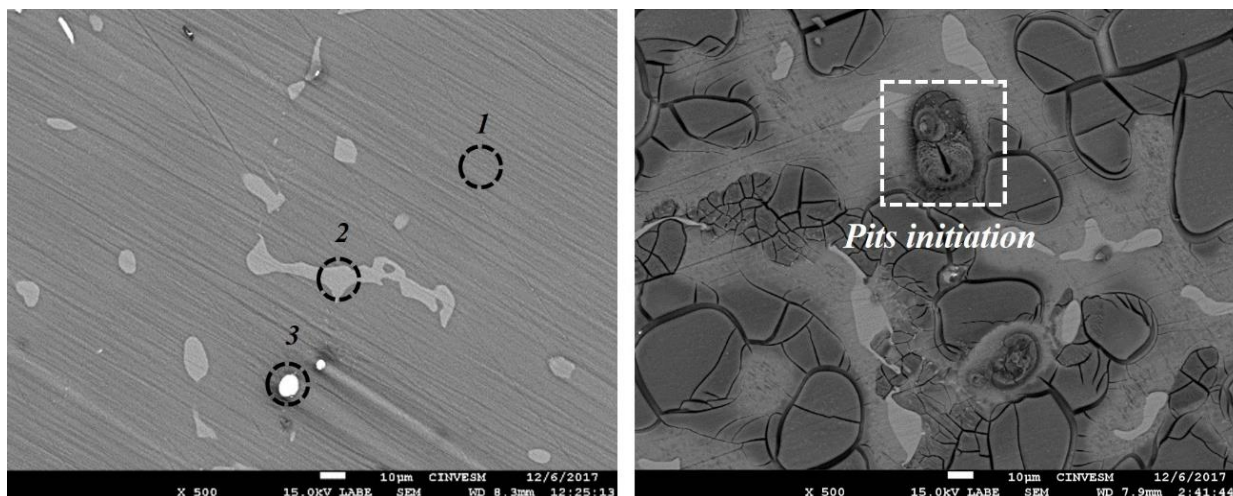

Figure 3. SEM images of freshly polished AZ91D surface (left), and after 2 h of immersion in SBF (right).

Table 1. EDS analysis (wt%) of specific zones shown in Figure 3 (a)

Zone	1	2	3
Mg	89.47	63.29	55.01
Al	08.69	33.26	26.63
Zn	00.96	2.79	-
Mn	-	-	17.71
O	0.88	00.66	00.65
Related phase	α	β	Al_8Mn_5

According to EDS quantification, zone 1 corresponds to the α-matrix of AZ91D alloy. The high content of Al in zone 2 is in agreement with the presence of β-phase ($Mg_{17}Al_{12}$) on the alloy surface, whereas, the white particle observed in zone 3 had an Al/Mn ratio which could be attributed to the aluminum-manganese phase, Al_8Mn_5 [13,42]. After 2 h of AZ91D exposure to SBF, it can be seen (Figure 3b) that the first pit nucleation occurs, as detected *in situ* by feedback mode (Figure 2). Correlating this SEM-EDS information with SECM feedback maps and optical images, it can be considered that the pitting corrosion occurs near the β-phase ($Mg_{17}Al_{12}$), which acts as a potent cathode owing to its less negative potential compared to that of the α-matrix [43,44].

3.3 Substrate generation /tip collection mode

As mentioned before, the SG/TC SECM mode was applied to map the hydrogen released from AZ91D alloy surface. Figure 4 presents SG/TC maps of the substrate, immersed in SBF solution, recorded at short times of exposure.
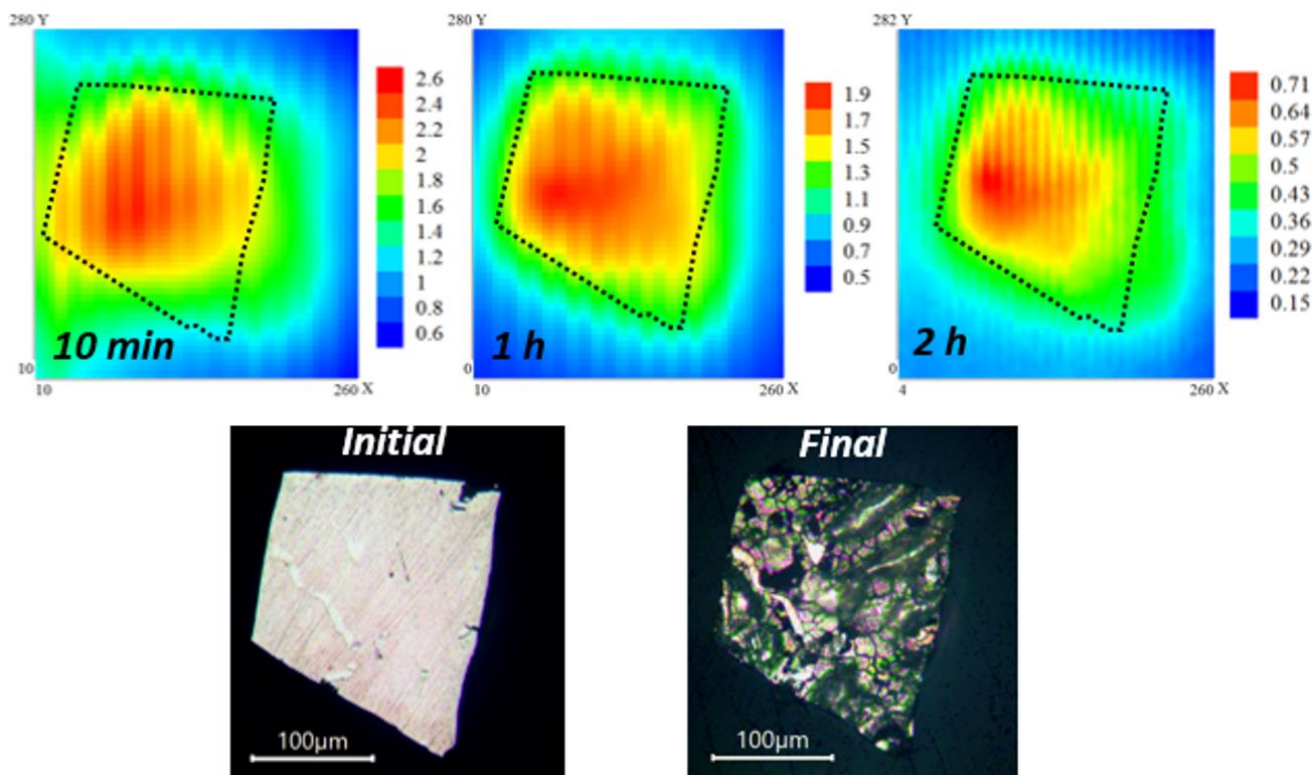

Figure 4. Top: SG/TC mode maps of AZ91D in SBF recorded with the platinum microelectrode (set at -0.05 V) at different exposure times. Scan dimensions: 260 μm x 280 μm. Color scales are in nA. Dotted outline on maps indicates metal-insulator border. Bottom: Optical images before and after experiment.

The changes in current (upper and lower color scale) is an indication of different hydrogen evolution intensity. However, the maps do not reveal a well-defined localized behavior, thereby the current response acquired reflects the contribution of the entire surface. This occurs because the H_2 gas diffuses rapidly toward the Pt sensor. The current values measured at 10 min, 1 h, and 2 h indicate that the hydrogen evolution intensity is higher at the beginning of the experiments and decreases over time. This behavior may be attributed to the early formation of a magnesium oxi-hydroxide film over AZ91D surface exposed to SBF [9,45]. It has been demonstrated that phosphate-containing solutions, like SBF, can induce passivation on AZ91D alloy [46,47]. Thus, even when pits are nucleating at AZ91D surface, a protective film seems to exist that covers the surrounding matrix and leads to a time-dependent decrease of hydrogen evolution.

4. CONCLUSIONS

Scanning electrochemical microscopy was successfully employed to characterize the initial corrosion activity of AZ91D Mg alloy at short periods of immersion in simulated body fluid. The maps obtained in feedback mode and the SEM images showed that after 2 h of experiments, the first pits were detected on the AZ91D substrate. This pitting behavior was associated to micro-galvanic corrosion, which was observed near the β-phase ($Mg_{17}Al_{12}$). Also, the SG/TC mode maps indicated a higher H_2 evolution flux at the beginning of the experiments, which diminished over time, indicating the possible early formation of a film of corrosion products.

It was demonstrated that SECM is a suitable option to contribute to increased information on the localized corrosion of AZ91D Mg alloy in physiological environments at real time.

References

1. F. Witte, N. Hort, C. Vogt, S. Cohen, K. U. Kainer, R. Willumeit, F. Feyerabend, *Curr. Opin. Solid State Mater. Sci.*, 12 (2008) 63.
2. W-D. Mueller, M. L. Nascimento, M. F. L De Mele, *Acta Biomater.*, 6 (2010) 1749.
3. N. T. Kirkland, N. Birbilis, M. P. Staiger, *Acta Biomater.*, 8 (2012) 925.
4. M. Esmaily, J. Svensson, S. Fajardo, N. Birbilis, G. Frankel, S. Virtanen, R. Arrabal, S. Thomas, L. Johansson, *Prog. Mater. Sci.*, 89 (2017) 92.
5. Y. Xin, T. Hu, P. Chu, *Acta Biomater.*, 7 (2011) 1452.
6. F. Witte, H. Ulrich, M. Rudert, E. Willbold, *J. Biomed. Mater. Res., Part* A, 81 (2007) 748.
7. F. Witte, H. Ulrich, C. Palm, E. Willbold, *J. Biomed. Mater. Res., Part* A, 81 (2007) 757.
8. F. Witte, V. Kaese, H. Haferkamp, E. Switzer, A. Meyer-Lindenberg, C. J. Wirth, H. Windhagen, *Biomaterials*, 26 (2005) 3557.
9. Y. Xin, C. Liu, X. Zhang, G. Tang, X. Tian, P. K. Chu, *J. Mater. Res.*, 22 (2007) 2004.
10. R. Zeng, W. Dietzel, F. Witte, N. Hort, C. Blawert, *Adv. Eng. Mater.*, 10 (2008) B3.
11. G. Song, *Adv. Eng. Mater.*, 7 (2005) 563.
12. R-C. Zeng, J. Zhang, W-J. Huang, W. Dietzel, K. Kainer, C. Blawert, K. Wei, *Trans. Nonferrous Met. Soc. China*, 16 (2006) s763.
13. G. Song, A. Atrens, M. Dargusch, *Corros. Sci.*, 41 (1998) 249.
14. A-M. Lafront, W. Zhang, S. Jin, R. Tremblay, D. Dubé, E. Ghali, *Electrochim. Acta*, 51 (2005) 489.
15. G. Song, A. Atrens, X. Wu, B. Zhang, *Corros. Sci.*, 40 (1998) 1769.
16. N. Aung, W. Zhou, *J. Appl. Electrochem.*, 32 (2002) 1397.
17. D. O. Wipf, *Colloids Surf.*, A, 93 (1994) 251.
18. R. M. Souto, S. Lamaka, S. González, Uses of scanning electrochemical microscopy in corrosion research, In: A. Méndez-Vilas and J. Díaz (Eds.) Microscopy: Science, technology, applications and education, Formatex, Vol. 3, (2010) Spain, 1769.

19. M. B. Jensen, D. E. Tallman, Application of SECM in corrosion research. In: A. J. Bard and M. V. Mirkin (Eds.) Scanning Electrochemical Microscopy, CRC Press, 2nd Ed., (2012) New York, 451.
20. N. A. Payne, L. I. Stephens, J. Mauzeroll, *Corrosion,* 73 (2017) 759.
21. S. Thomas, J. Izquierdo, N. Birbilis, R. M. Souto, *Corrosion*, 71 (2014) 171.
22. R. M. Souto, A. Kiss, J. Izquierdo, L. Nagy, I. Bitter, G. Nagy, *Electrochem. Commun*., 26 (2013) 25
23. U. M. Tefashe, M. E. Snowden, P. Dauphin-Ducharme, M. Danaie, G. A. Botton, J. Mauzeroll, *J. Electroanal. Chem*., 720 (2014) 121.
24. W. Liu, F. Cao, Y. Xia, L. Chang, J. Zhang, *Electrochim. Acta*, 132 (2014) 377.
25. J. Izquierdo, L. Nagy, I. Bitter, R. M. Souto, G. Nagy, *Electrochim. Acta*, 87 (2013) 283.
26. P. Dauphin-Ducharme, R. M. Asmussen, U. M. Tefashe, M. Danaie, W. J. Binns, P. Jakupi, G. A. Botton, D. W. Shoesmith, J. Mauzeroll , *J. Electrochem. Soc*., 161 (2014) C557.
27. R. M. Asmussen, W. J. Binns, P. Jakupi, P. Dauphin-Ducharme, U. M. Tefashe, J. Mauzeroll, D. Shoesmith, *Corros. Sci*., 93 (2015) 70.
28. P. Dauphin-Ducharme, C. Kuss, D. Rossouw, N. A. Payne, L. Danis, G. A. Botton, J. Mauzeroll, *Electrochem. Soc*., 162 (2015) C677.
29. S. S. Jamali, S. E. Moulton, D. E. Tallman, M. Forsyth, J. Weber, G. G. Wallace, *Electrochim. Acta*, 152 (2015) 294.
30. P. Dauphin-Ducharme, R. M. Asmussen, D. W. Shoesmith, J. Mauzeroll, *J. Electroanal. Chem*., 736 (2015) 61.
31. J. Izquierdo, B. M. Fernández-Pérez, D. Filotás, Z. Őri, A. Kiss, R. T. Martín-Gómez, L. Nagy, G. Nagy, R. M. Souto, *Electroanalysis*, 28 (2016) 2354.
32. Y. Xia, Z. Zhu, L. Chang, J. Zhang, F. Cao, J. Zhang, *Int. J. Electrochem. Sci*., 12 (2017) 2145
33. A. Oyane, H. M. Kim, T. Furuya, T. Kokubo, T. Miyazaki, T. Nakamura. *J. Biomed. Mater. Res., Part A*, 65 (2003) 188.
34. M. P. Staiger, A. M. Pietak, J. Huadmai, G. Dias, *Biomaterials*, 27 (2006) 1728.
35. X. Gu, Y. Zheng, L. Chen, *Biomed. Mater*., 4 (2009) 065011
36. Y. Xin, T. Hu, P. K. Chu, *J. Electrochem. Soc*., 157 (2010) C238
37. S. S. Jamali, S. E. Moulton, D. E. Tallman, M. Forsyth, J. Weber, G. G. Wallace, *Corros. Sci.,* 86 (2014) 93.
38. M. A. Alpuche-Aviles, D. O. Wipf, *Anal. Chem*., 73 (2001) 4873.
39. F-R. F. Fan, C. Demaille, The preparation of tips for scanning electrochemical microscopy. In: A. J. Bard, M. V. Mirkin (Eds.) Scanning Electrochemical Microscopy. Marcel Dekker, Inc., (2001) New York, 75.
40. T. J. Smith, K. J. Stevenson, Reference electrodes. In: C. G. Zoski (Ed.) Handbook of electrochemistry, Elsevier, (2006) Amsterdam, 92.
41. R. Ambat, N. N. Aung, W. Zhou, *J. Appl. Electrochem*., 30 (2000) 865.
42. R. Ambat, N. N. Aung, W. Zhou, *Corros. Sci*., 42 (2000) 1433.
43. G. Song, A. Atrens, *Adv. Eng. Mater*., 5 (2003) 837.
44. O. Lunder, K. Nisancioglu, R. S. Hansen, Corrosion of die cast magnesium-aluminum alloys. SAE Technical Paper (1993).
45. D. Gopi, P. Bhalaji, S. Ramya, L. Kavitha, *J. Ind. Eng. Chem*. 23 (2015) 218.
46. F. E-T. Heakal, A. M. Fekry, M. Z. Fatayerji, *J. Appl. Electrochem*., 39 (2009) 583
47. F. E-T. Heakal, A. M. Fekry, M. Z. Fatayerji, *J. Appl. Electrochem*., 39 (2009) 1633